Variation of acoustic energy at low frequencies across sudden area expansions sustaining a subsonic flow

Renaud Gaudron*, Juan Guzmán Iñigo† and Aimee S. Morgans‡
Imperial College London, UK

The acoustic energy balance of a sudden area expansion is known to be altered in the presence of a mean flow. In this work, Ronneberger's quasi-steady model describing the acoustic response of a sudden area expansion sustaining a subsonic mean flow of arbitrary Mach number is revisited using the acoustic absorption coefficient, shown to be a function of the inlet Mach number M_u, cross section area ratio θ, and upstream acoustic reflection coefficient $\mathcal{R}_u$. These analytical predictions are tested using a two-step numerical strategy, whereby the mean flow variables are obtained using RANS simulations and the fluctuating variables are computed using in-house Linearised Navier-Stokes Equations solvers. The agreement between the analytical model and the numerical results is found to be excellent for all geometries, mean flows, and acoustic boundary conditions investigated. The generation of acoustic energy by the flow expansion is observed analytically and numerically for high Mach number flows undergoing a slight sudden area increase for given acoustic boundary conditions. Conversely, it is found that substantial acoustic energy damping occurs across sudden area expansions characterised by a wide range of parameters $(M_u, \theta, \mathcal{R}_u)$. Moreover, entropy and vorticity fluctuations are found to be generated at the sudden area expansion but entropy fluctuations are shown to have a negligible impact on the acoustic response of the area expansion at low and intermediate Mach numbers. Finally, the analytical model is found to be reasonably accurate up to Helmholtz numbers He $\sim 0.05 - 0.1$, corresponding to the frequency range of many industrial applications.

I. Introduction

The production and damping of acoustic energy across sudden cross section area expansions sustaining a subsonic mean flow is of interest in many industrial applications. These range from predicting the noise of ventilation ducts [1] and other industrial duct networks [2, 3] to assessing the efficiency of internal combustion engine exhaust silencers [2, 4] and predicting the onset, growth and saturation of thermoacoustic modes in gas turbines [5, 6].

*Research Associate, Department of Mechanical Engineering, r.gaudron@imperial.ac.uk
†Research Associate, Department of Mechanical Engineering, j.guzman-inigo@imperial.ac.uk
‡Professor, Department of Mechanical Engineering, a.morgans@imperial.ac.uk

The acoustic response of sudden area expansions sustaining a subsonic mean flow was originally described using quasi-steady models [4, 7–9]. In these models, the conservation of mass, momentum, and energy are linearised and integrated over a control volume enclosing the sudden area expansion. The mean flow in the downstream duct is either assumed to expand [3, 4, 7, 9] or form a jet of constant width [8, 10]. Three types of waves may coexist in the presence of a mean flow: acoustic waves, entropy waves and vorticity waves [11]. Acoustic waves are irrotational isentropic waves propagating at the speed of sound [12, 13] while entropy and vorticity waves are respectively irrotational isobaric and isentropic isobaric waves convected by the mean flow [11, 13]. These waves are independent in a steady uniform flow but may interact with each other in more complex flows [9, 11, 14]. For instance, entropy and vorticity waves are generated when acoustic waves impinge on a sudden area expansion with large-scale flow separation [4, 7, 9]. Ronneberger's model is widely recognised as the most advanced quasi-steady model because it accounts for entropy and vorticity wave generation, as well as the presence of a mean entropy jump, corresponding to a stagnation pressure loss, across the area expansion [7, 9, 15].

Quasi-steady models describing the acoustic scattering at sudden area expansions are limited to relatively low frequencies, and more recent investigations have aimed to include frequency-dependent effects [1, 16–20]. Vortex-sound interactions were either described using a Wiener-Hopf technique with a Kutta condition applied at the rim of the area expansion [1, 18, 21] or as a source/sink term in the wave equation, subsequently solved using Green's functions [16, 19, 20, 22]. Alternatively, the scattering of sound across sudden area expansions was modelled using a multimodal method [17, 23]. These frequency-dependent models are notably more complex than their quasi-steady counterparts and additional assumptions about the mean flow and/or fluctuating variables are usually required. For instance, the generation of entropy waves across the area expansion is commonly neglected [1, 16–23] and the mean flow is sometimes assumed to have a low Mach number [16, 19, 20, 22].

The acoustic scattering of sudden area expansions was also characterised experimentally at low and intermediate Mach numbers [7, 9, 15, 16, 24, 25]. Ronneberger's datasets date back to the 1960s-1980s but are still the most comprehensive and are thus used in many recent numerical [26–28], analytical [17, 18], and experimental [29] studies. Conversely, numerical investigations are relatively recent and based on either the CFD/SI approach [27, 30] or the two-step CFD approach [26, 28, 31]. In the CFD/SI approach, the mean and fluctuating variables are obtained simultaneously using URANS simulations [30] or Large-Eddy simulations [27]. The acoustic response of the sudden area expansion is then extracted using System Identification (SI) techniques. In the two-step CFD approach, the mean flow is first obtained using RANS simulations [28, 31] or Large-Eddy simulations [26]. The fluctuating variables are then obtained using either a Linearised Navier-Stokes Equations (LNSE) solver [26, 28, 31] or a Linearised Euler Equation (LEE) solver [26]. In theory, both approaches can be used to characterise the acoustic response of sudden

area expansions containing a (subsonic) compressible mean flow. In practice, several numerical difficulties arise at intermediate and high Mach numbers [28, 32], and the existing numerical studies focus on low Mach number flows only [26–28, 30]. It was established in these numerical studies that the acoustic response of sudden area expansions is almost frequency-independent at low Helmholtz numbers [26–28].

A subsonic flow passing through a sudden area contraction (or a slowly-varying area change) can be assumed to be isentropic [4, 33, 34]. In that case, the production or damping of acoustic energy across the area change is negligible [34]. Conversely, a subsonic flow going through a sudden area expansion is not isentropic because of large-scale flow separation occurring at the rim of the area expansion [4, 9, 34]. Acoustic energy may then be damped or generated in the shear layers and recirculation zones downstream of the area expansion. The amount of damping or generation can be quantified using an acoustic energy balance [6, 35]. An expression for the acoustic energy balance in the presence of a subsonic mean flow was first established for an homentropic irrotational flow [36]. The concept of acoustic energy was then extended to non-uniform flows, and a corresponding expression for the acoustic energy balance was derived [37]. This expression was further extended to arbitrary steady flows in a later article [14]. The source terms in a macroscopic acoustic energy balance fully characterise the generation and damping of acoustic energy across any given geometry. However, estimating these source terms is intricate because time-averaged surface and volume integrals need to be computed [6, 38]. An alternative formalism based on the acoustic absorption coefficient can be used to estimate these source/sink terms for a given geometry by either determining the acoustic energy generation/damping potentiality [39, 40] or by directly computing the acoustic energy generation/damping for given acoustic boundary conditions [6, 21, 22, 34].

The main objective of this study is to characterise the damping and generation of acoustic energy across sudden area expansions sustaining a subsonic mean flow using analytical and numerical strategies. Both approaches are applied to a variety of configurations covering a wide range of expansion ratios, subsonic Mach numbers (including high Mach numbers), and acoustic boundary conditions. Section II contains the derivation of an analytical model predicting the acoustic absorption coefficient of a sudden area expansion containing a subsonic flow. The mean and linearised jump conditions across the area expansion are obtained by following Ronneberger's quasi-steady approach and are then combined with a generalised expression of the acoustic absorption coefficient obtained for arbitrary boundary conditions. Numerical simulations based on the two-step CFD approach are then introduced in Sec. III to assess the accuracy of the analytical model at low, intermediate, and high Mach numbers. The mean flow variables are first obtained using RANS simulations. The fluctuating variables are then determined using in-house Linearised Navier-Stokes Equations solvers with eddy viscosity, including for flow conditions at high Mach numbers for the first time. The flow and geometry conditions giving rise to acoustic damping and generation are analysed. Finally, the impact of the Helmholtz number

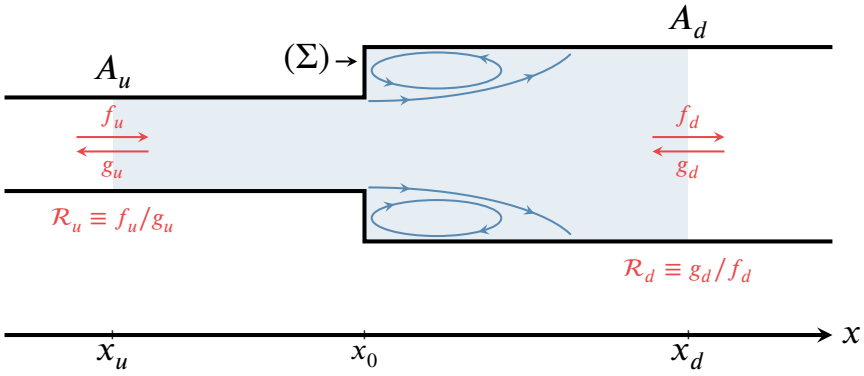

Fig. 1 **Sketch representing a sudden area expansion sustaining a subsonic mean flow.**

on the acoustic response of the area expansion is investigated numerically to assess the accuracy of the model as the frequency is increased.

II. Quasi-steady analytical model

The scope of this work is limited to the absorption and generation of acoustic energy across an axisymmetric sudden cross section area expansion sustaining a high-Reynolds number subsonic mean flow. The configuration considered is sketched in Fig. 1. A perfect gas flows from left to right. Three reference locations are defined: x_u (respectively x_d) corresponding to the inlet (respectively outlet) of the geometry and x_0 corresponding to the location where the cross section area A suddenly increases. Without loss of generality, x_0 will be set to zero in the following derivations. The subscripts u, d and 0 are used to denote variables assessed at these reference locations. Each physical variable y is then decomposed into a mean $\overline{y}$ and a fluctuating y' variable such that $y' \ll \overline{y}$, with the exception of velocity, where the previous inequality is replaced by $u' \ll \overline{c}$ where u' is the velocity fluctuation and $\overline{c}$ is the sound speed.

A. Mean flow

Axisymmetric sudden cross section area expansions containing a high-Reynolds number subsonic mean flow have been characterised extensively using analytical models [41, 42], experiments [42–46], and numerical simulations [42, 45, 47, 48]. The corresponding mean flow topology is thus well-known. First, large-scale flow separation occurs at the rim of the sudden area expansion, thus forming a turbulent free shear layer. Recirculation zones are generated between the walls and the shear layer, which bends towards the wall due to a slight pressure difference across it. At a certain distance from the area expansion, the shear layer reattaches to the wall. This mean flow is not isentropic because of viscous dissipation occurring in the shear layer and recirculation zones [4, 9].

Neglecting body forces, thermal conduction and thermal radiation, the mean conservation of mass, momentum and

stagnation enthalpy are given by:

$$\nabla \cdot (\overline{\rho}\, \overline{\mathbf{u}}) = 0 \tag{1}$$

$$\nabla \cdot (\overline{\rho}\, \overline{\mathbf{u}} \otimes \overline{\mathbf{u}}) = -\nabla\, \overline{p} \tag{2}$$

$$\nabla \cdot \left(\overline{\rho}\, \overline{\mathbf{u}}\, \overline{H}\right) = 0 \tag{3}$$

where $\overline{\rho}$, $\overline{\mathbf{u}}$, $\overline{p}$, and $\overline{H}$ are the mean density, mean velocity, mean pressure, and mean stagnation enthalpy respectively. Following the typical procedure [9, 41], those conservation equations are then integrated over the control volume corresponding to the region located between x_u and x_d, as represented in light blue in Fig. 1, thus yielding the following dimensionless equations:

$$M_d\, \Xi\ = \alpha \theta M_u \tag{4}$$

$$1 + \gamma M_d^2 = \alpha \left(1 + \theta \gamma M_u^2\right) \tag{5}$$

$$1 -\ \Xi^2\ = \frac{\gamma - 1}{2} (M_u^2\, \Xi^2\ - M_d^2) \tag{6}$$

where γ is the adiabatic index, M_u and M_d are the inlet and outlet Mach numbers, $\theta = A_u/A_d$ is the cross section area ratio, $\alpha = \overline{p}_u/\overline{p}_d$ is the mean pressure ratio and $\Xi = \overline{c}_u/\overline{c}_d$ is the mean sound speed ratio. Eqs. (4)-(6) are obtained assuming that all mean flow variables are one-dimensional at x_u and x_d. Equation (5) is obtained by further assuming that the mean pressure on the vertical wall (Σ) is equal to the mean pressure just before the area expansion [3, 8, 9, 41]. This assumption will be discussed in Sec. III. Equations (4)-(6) can be solved numerically for any given set of two dimensionless parameters, chosen here as M_u and θ, and are equivalent to those derived by Batchelor [41] and Ronneberger [7, 9, 15].

B. Fluctuating variables

It is now assumed that acoustic waves and entropy waves are present on each side of the area expansion. Furthermore, acoustic and entropy fluctuations are assumed to be plane waves for $x \leq x_u$ and $x \geq x_d$ respectively. In these two regions, the Riemann invariant associated with the acoustic wave propagating in the flow direction (respectively opposite to the flow direction) is denoted by f (respectively g). It is assumed that the domain located between x_u and x_d is acoustically and hydrodynamically compact, i.e. that the frequency is low enough such that wave propagation between x_u and x_d is negligible. This assumption is also called the quasi-steady assumption. Under the previous assumptions, the upstream acoustic pressure p'_u and upstream acoustic velocity u'_u are then simply expressed in terms of the corresponding Riemann invariants f_u and g_u [49]. Similar expressions are also derived for p'_d and u'_d in terms of f_d and g_d. A link between the

upstream and downstream variables is then established by considering the linearised conservation of mass, momentum and stagnation enthalpy, given by:

$$\nabla \cdot (\rho' \, \overline{\mathbf{u}} + \overline{\rho} \, \mathbf{u}') = 0 \tag{7}$$

$$\nabla \cdot (\rho' \, \overline{\mathbf{u}} \otimes \overline{\mathbf{u}} + \overline{\rho} \, \mathbf{u}' \otimes \overline{\mathbf{u}} + \overline{\rho} \, \overline{\mathbf{u}} \otimes \mathbf{u}') = -\nabla \, p' \tag{8}$$

$$\nabla \cdot \left(\rho' \, \overline{\mathbf{u}} \, \overline{H} + \overline{\rho} \, \mathbf{u}' \, \overline{H} + \overline{\rho} \, \overline{\mathbf{u}} \, H'\right) = 0 \tag{9}$$

where ρ', $\mathbf{u}'$, p', and H' are the density, velocity, pressure, and stagnation enthalpy fluctuations respectively. Those equations are then rearranged, simplified, and integrated over the control volume corresponding to the region located between x_u and x_d. This approach was introduced by Ronneberger in a series of works [7, 9, 15]. The common assumption that the fluctuating pressure on (Σ) is equal to the fluctuating pressure just before the area expansion is used to close the model [4, 8, 9]. This assumption will be discussed in Sec. III. The corresponding expressions are then further simplified using Eqs. (4)-(6), thus leading to:

$$\begin{bmatrix} f_d \\ g_u \\ \tilde{s}'_d \end{bmatrix} = \underbrace{\begin{bmatrix} \alpha(1+M_d) & M_d(M_u^{-1}-1) & -\alpha M_d \\ \alpha(1+M_d)^2 & M_d\Xi(2-M_u)-\alpha & -\alpha M_d^2 \\ \alpha(1+M_d) & \Xi^2(M_u-1) & \alpha/(\gamma-1) \end{bmatrix}^{-1} \begin{bmatrix} M_d(1+M_u^{-1}) & \alpha(1-M_d) & -M_d \\ M_d\Xi(2+M_u)+\alpha & -\alpha(1-M_d)^2 & -M_dM_u\Xi \\ (1+M_u)\Xi^2 & \alpha(M_d-1) & \Xi^2/(\gamma-1) \end{bmatrix}}_{\mathbf{A}} \begin{bmatrix} f_u \\ g_d \\ \tilde{s}'_u \end{bmatrix} \tag{10}$$

where $\tilde{s}'_j = s'_j \overline{\rho}_j \overline{c}_j^2 / c_p$ (for $j = u, d$) re-scales the entropy fluctuations to have the same dimension as f_j and g_j, i.e. Pa. Equation (10) fully describes the response of a sudden area expansion to incoming acoustic and entropy waves. The focus of this study being on acoustic waves, $\tilde{s}'_u$ is further set to zero, but entropy waves are still generated at the sudden area expansion, i.e. $\tilde{s}'_d \neq 0$ [4, 8]. In that case, the acoustic response of the sudden area expansion is fully characterised by the Scattering Matrix (or S-matrix) $\mathbf{S}$, corresponding to the first two rows and columns of $\mathbf{A}$. The impact of incoming entropy waves on the response of sudden area expansions has been investigated in separate works [31, 32].

C. Acoustic absorption coefficient

The acoustic absorption coefficient Δ corresponding to the region located between x_u and x_d is defined as[6, 21, 22]:

$$\Delta = 1 - \frac{|W_d^+| + |W_u^-|}{|W_u^+| + |W_d^-|} \tag{11}$$

where $W_j^{\pm}$ is the time-averaged surface-averaged acoustic energy flux associated with the wave propagating in the

positive/negative direction at x_u (for $j = u$) or x_d (for $j = d$). The acoustic absorption coefficient compares the average amount of acoustic energy entering and leaving the geometry. There is no outgoing acoustic energy on average for $\Delta = 1$. The relative amount of outgoing acoustic energy then increases as the acoustic absorption coefficient decreases, until it becomes equal to the amount of incoming acoustic energy for $\Delta = 0$. Finally, there is more acoustic energy leaving the control volume than entering it on average for $\Delta < 0$. A further decrease in the acoustic absorption coefficient corresponds to proportionally more outgoing acoustic energy. There is a strong link between this definition of the acoustic absorption coefficient and the notion of acoustic energy sink/source. The local time-averaged acoustic energy balance at low frequencies is given by [14, 37]:

$$\nabla \cdot I = -\mathcal{D} \tag{12}$$

where I is the time-averaged acoustic energy flux and $\mathcal{D}$ is the time-averaged acoustic energy sink per unit volume (which can be a source if $\mathcal{D} < 0$). In this study, $\mathcal{D}$ is defined using Myers' approach [14] and contains terms corresponding to the conversion of sound into mean and perturbed vorticity only. When integrated over the control volume corresponding to the light blue region in Fig. 1, Eq. (12) shows that characterising the acoustic energy source/sink between x_u and x_d or the time-averaged surface-averaged acoustic energy fluxes at x_u and x_d is fully equivalent. The acoustic absorption coefficient can thus be used to determine if the sudden cross section area expansion acts as a source ($\Delta > 0$) or a sink ($\Delta < 0$) of acoustic energy [6]. The acoustic absorption coefficient can also be used to quantify the strength of the acoustic energy attenuation (or generation) across the area expansion. Physically, the corresponding surplus of acoustic energy is extracted from the mean flow and/or from a different type of perturbation [11, 37]. The expressions of the time-averaged surface-averaged acoustic energy fluxes in an arbitrary flow are available in the literature [14]. Equation (11) can thus be recast into the following equations by assuming that the flow is irrotational at x_u and x_d (but not necessarily inside the domain)[6, 34]:

$$\Delta = 1 - \frac{(1+M_d)^2 |f_d|^2 + \theta\Xi\alpha^{-1}(1-M_u)^2 |g_u|^2}{\theta\Xi\alpha^{-1}(1+M_u)^2 |f_u|^2 + (1-M_d)^2 |g_d|^2} \tag{13a}$$

$$= 1 - \frac{(1+M_d)^2 |\mathbf{S}_{12} + \mathcal{R}_u \det\mathbf{S}|^2 + \theta\Xi\alpha^{-1}(1-M_u)^2 |\mathbf{S}_{22}|^2}{\theta\Xi\alpha^{-1}(1+M_u)^2 |\mathcal{R}_u\mathbf{S}_{22}|^2 + (1-M_d)^2 |1-\mathcal{R}_u\mathbf{S}_{21}|^2} \tag{13b}$$

$$= 1 - \frac{(1+M_d)^2 |\mathbf{S}_{11}|^2 + \theta\Xi\alpha^{-1}(1-M_u)^2 |\mathbf{S}_{21} + \mathcal{R}_d \det\mathbf{S}|^2}{\theta\Xi\alpha^{-1}(1+M_u)^2 |1-\mathcal{R}_d\mathbf{S}_{12}|^2 + (1-M_d)^2 |\mathcal{R}_d\mathbf{S}_{11}|^2} \tag{13c}$$

Equation (13a) shows that the variation of acoustic energy across the sudden area expansion depends on: 1) five dimensionless parameters characterising the mean flow, and 2) the amplitudes of the Riemann invariants on each side of the area expansion. Since the Riemann invariants at x_u and x_d are functions of the acoustic response of the area expansion and its acoustic environment, Eq. (13a) shows that the acoustic absorption coefficient characterises both

of them simultaneously. Equation (13a) generalises previous expressions obtained with more restrictive assumptions [16, 20, 22]. Equation (13a) can also be expressed in terms of the coefficients of the Scattering Matrix and the upstream acoustic pressure reflection coefficient $\mathcal{R}_u = f_u/g_u$, corresponding to Eq. (13b), or the downstream acoustic pressure reflection coefficient $\mathcal{R}_d = g_d/f_d$, corresponding to Eq. (13c). In this work, the upstream and downstream acoustic reflection coefficients represent the impact of the elements placed upstream and downstream of the area expansion and are not coefficients of the Scattering Matrix. Equations 13a)-Eq. (13c) are equivalent and can be obtained from one another. For instance, Eq. (13c) can be obtained from Eq. (13b) by expressing $\mathcal{R}_u$ as a function of $\mathcal{R}_d$ using the following characteristic equation:

$$\mathbf{S}_{11}\mathbf{S}_{22}\mathcal{R}_u\mathcal{R}_d = (1 - \mathbf{S}_{21}\mathcal{R}_u)\,(1 - \mathbf{S}_{12}\mathcal{R}_d) \tag{14}$$

More details about the derivations of Eqs. (13a)-(13c) can be found in [6, 34]. Combining Eqs. (4)-(6) with Eq. (10) and Eq. (13b) - or equivalently Eq. (13c) -, the acoustic absorption coefficient of an area expansion is shown to be a function of three independent parameters: two dimensionless numbers characterising the mean flow and a boundary acoustic reflection coefficient. The inlet Mach number M_u, cross section area ratio θ and upstream acoustic reflection coefficient $\mathcal{R}_u$ will be used in the remainder of this study.

Previous studies used the Scattering Matrix to determine the extremal values of the ratio of the dissipated/generated acoustic energy over the incident acoustic energy for all possible acoustic boundary conditions [39]. The corresponding criterion depends solely on the properties of the acoustic element but does not give a quantitative estimate of the amount of acoustic energy dissipated for given acoustic boundary conditions. The approach presented in this study is different as it provides the exact amount of acoustic energy dissipation/generation (with respect to the incident acoustic energy) for given acoustic boundary conditions but does not analyse the potential for acoustic energy dissipation/generation over all possible acoustic states.

Explicit expressions for the acoustic absorption coefficient in the low Mach number regime can be derived by neglecting terms of order higher than M_u in Eqs. (4)-(6), Eq. (10), and Eqs. (13b)-(13c), thus yielding:

$$\Delta = \frac{4\theta(\theta-1)^2}{(\theta+1)} \frac{|\mathcal{R}_u - 1|^2}{|\mathcal{R}_u + 1|^2 + \theta|\mathcal{R}_u - 1|^2} M_u \tag{15a}$$

$$= \frac{4(\theta-1)^2}{(\theta+1)} \frac{|1 - \mathcal{R}_d|^2}{\theta|1 + \mathcal{R}_d|^2 + |1 - \mathcal{R}_d|^2} M_u \tag{15b}$$

Equations (15a)-(15b), which can be used interchangeably, predict that the acoustic absorption coefficient initially

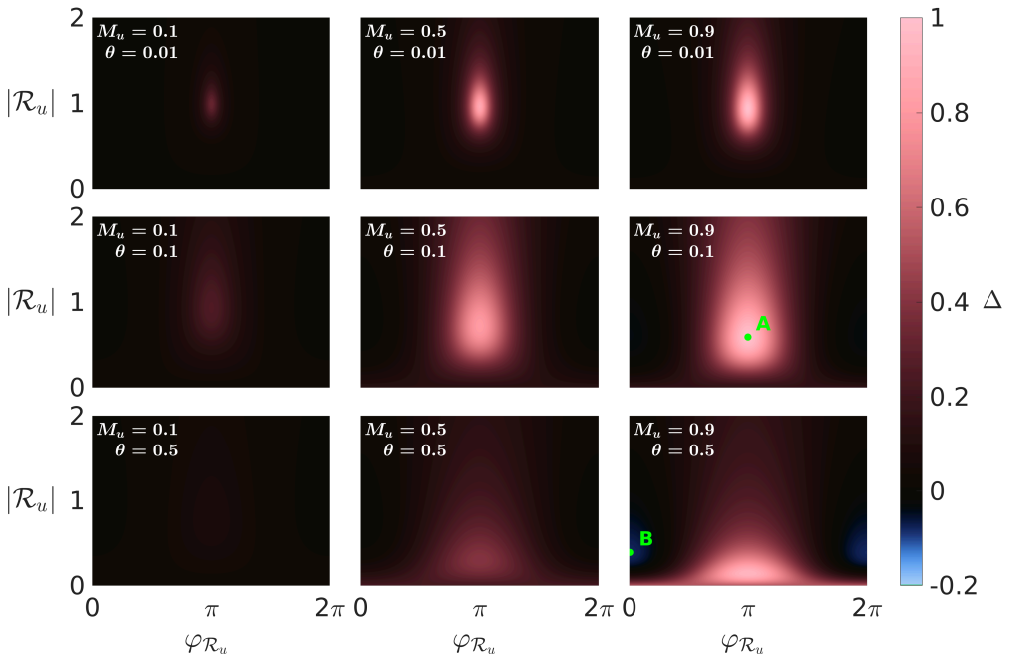

Fig. 2 Acoustic absorption coefficient of a sudden area expansion as a function of the modulus (y-axis) and phase (x-axis) of the upstream acoustic reflection coefficient for three different upstream Mach numbers and cross section area ratios. (Top) $\theta = 0.01$**. (Center)** $\theta = 0.1$**. (Bottom)** $\theta = 0.5$**. (Left)** $M_u = 0.1$**. (Middle)** $M_u = 0.5$**. (Right)** $M_u = 0.9$**. Point A corresponds to (**$M_u = 0.9$**,** $\theta = 0.1$**,** $\mathcal{R}_u = -0.59$**). Point B corresponds to (**$M_u = 0.9$**,** $\theta = 0.5$**,** $\mathcal{R}_u = 0.39$**). Acoustic energy is generated for** $\Delta < 0$ **corresponding to a blue hue.**

increases linearly with the upstream Mach number. In the absence of a mean flow, the acoustic absorption coefficient becomes zero since the damping and generation of acoustic energy across the area expansion comes from the coupling between the acoustic waves and vortical waves that are convected by the mean flow [16, 21, 28, 50]. Another mechanism that could lead to a non-zero acoustic absorption coefficient in the absence of a mean flow is acoustically excited vortex shedding. This phenomenon is negligible here because of viscous effects at the rim of the area expansion and because the amplitude of perturbations is assumed to be small enough [51, 52]. The deviation between the acoustic absorption coefficient predicted by the general model, given by Eqs. (4)-(6), Eq. (10), and Eq. (13b) and the low Mach number approximation, given by Eq. (15a) was found to be remain lower than 0.06 in the low Mach number regime ($M_u < 0.1$) whatever θ and $\mathcal{R}_u$, thus validating Eqs. (15a)-(15b).

D. Effect of the acoustic reflection coefficient

The impact of the modulus and phase of the upstream acoustic reflection coefficient on the acoustic absorption coefficient is investigated in Fig. 2. The mean flow and acoustic response of the area expansion are described using Eqs. (4)-(6) and Eq. (10) respectively. The acoustic absorption coefficient is then computed using Eq. (13b). Nine different cases are retained, corresponding to a large ($\theta = 0.01$), medium ($\theta = 0.1$) and small ($\theta = 0.5$) area expansion sustaining a low ($M_u = 0.1$), moderate ($M_u = 0.5$) or high ($M_u = 0.9$) Mach number flow. The values of the acoustic

absorption coefficient depicted in Fig. 2 are symmetric with respect to $\varphi_{\mathcal{R}_u} = \pi$. This observation is due to the symmetry properties of Eq. (13b) for real-valued Scattering Matrices.

Figure 2 demonstrates that the acoustic absorption coefficient is close to zero for $M_u = 0.1$ whatever the cross section area ratio and upstream reflection coefficient. As the Mach number increases, the impact of the reflection coefficient becomes progressively more important. At high Mach numbers, the upstream reflection coefficient determines if the incoming acoustic energy is partially damped ($0 < \Delta < 1$), entirely damped ($\Delta = 1$), or even amplified ($\Delta < 0$) across the area expansion, as can be seen for instance in Fig. 2-(Bottom Right), corresponding to $\theta = 0.5$ and $M_u = 0.9$. A region where the absorption coefficient is close to unity is found for moderate-to-high Mach numbers and for phases of the upstream reflection coefficient close to π. For instance, $\Delta = 0.994$ for $\theta = 0.1$, $M_u = 0.9$ and $\mathcal{R}_u = -0.59$, corresponding to Point A in Fig. 2-(Center Right). Conversely, a region where the absorption coefficient is negative is observed for small area expansions sustaining a high Mach number flow and for phases of the upstream reflection coefficient close to 0. For instance, $\Delta = -0.079$ for $\theta = 0.5$, $M_u = 0.9$ and $\mathcal{R}_u = 0.39$, corresponding to Point B in Fig. 2-(Bottom Right). The analytical model thus predicts that small area expansions will generate acoustic energy, and thus whistle, in the high Mach number regime for specific acoustic boundary conditions. Conversely, large area expansions with $\theta \ll 1$ are not prone to whistling according to the model.

III. Numerical simulations

The predictions according to the quasi-steady analytical model described in Sec. II will now be compared against numerical simulations for a large ($\theta = 0.01$), medium ($\theta = 0.1$) and small ($\theta = 0.5$) area expansion sustaining a low ($M_u = 0.1$), moderate ($M_u = 0.5$) and high ($M_u = 0.9$) Mach number flow. The mean flow variables have a significant impact on the acoustic response of the area expansion [25, 28] and it is thus essential to accurately capture the mean flow topology. On the other hand, the fluctuating variables are much smaller than the mean flow variables [2, 49, 53] and their influence on the mean flow topology can thus be neglected [28, 31, 54, 55]. As a consequence, a two-step CFD approach where the mean and fluctuating variables are determined sequentially will be used in this study. For each case, the mean flow variables are first obtained using a 3D Reynolds-Averaged Navier–Stokes (RANS) compressible solver with a $k - \omega$ SST turbulence model. The fluctuating variables are then determined using two in-house Linearised Navier-Stokes Equations (LNSE) solvers (with and without acoustic-entropy coupling). The numerical acoustic absorption coefficient is finally computed using both the mean and linearised flow simulations.

		θ		
		0.01	**0.1**	**0.5**
	0.1	5.80×10^5	1.39×10^5	2.67×10^4
$\mathbf{M_u}$	**0.5**	5.79×10^5	1.35×10^5	2.52×10^4
	0.9	5.76×10^5	1.27×10^5	2.19×10^4

Table 1 Reynolds number Re_H based on the step height for each configuration of interest.

A. Mean flow simulations

The first step is to obtain the mean flow for all nine configurations of interest. To this end, the compressible RANS equations are solved with the finite volume solver OpenFOAM version 7 [56]. Steady-state variables are obtained using a SIMPLE algorithm. The effects of turbulence are described using a $k - \omega$ shear-stress-transport (SST) turbulence model, well-adapted to wall-bounded flows [57].

The computational domain is a sequence of two concentric cylindrical wedges with a 5° angle. A single cell is used in the transverse direction and appropriate boundary conditions are applied on the associated walls, which makes the geometry 2D axisymmetric. Each duct has an axial extent of $50D_u$ where D_u is the diameter of the upstream duct. The diameter of the downstream duct is obtained from D_u and θ. The inlet (respectively outlet) is located at the extremity of the leftmost (respectively rightmost) duct. A uniform velocity profile corresponding to the desired Mach number is prescribed at the inlet. A constant temperature $\overline{T} = 273$ K and a zero-gradient condition for the pressure are also prescribed at the inlet. Conversely, a constant pressure $\overline{p} = 1.013 \times 10^5$ Pa and a zero-gradient condition for the velocity are imposed at the outlet. A slip boundary condition is applied on the lateral wall of the upstream duct, along with a zero-gradient condition for the temperature and pressure. This ensures that the mean flow variables remain uniform in the upstream duct, which greatly simplifies the post-processing procedure with negligible impact on numerical results at low frequencies, as demonstrated in a separate work [32]. Finally, a no-slip boundary condition along with a zero-gradient condition for the temperature and pressure is prescribed on all remaining boundaries. A structured mesh consisting of hexahedral elements is optimised for each set of upstream Mach number and cross section area ratio. The number of cells is comprised between 72,400 and 604,500 depending on the exact configuration, with more cells close to the area expansion, shear layer, and boundary layer in the downstream duct. Each mesh is designed such that $y^+ < 1$ at the downstream no-slip walls to fully resolve the viscous sublayer.

The Reynolds numbers $\mathrm{Re}_H = \overline{\rho}_u \overline{u}_u H/\mu$ based on the step height $H = (D_d - D_u)/2$ are summarised in Tab. 1 for each configuration of interest. These Reynolds numbers are comparable to those of previous studies [42, 44–46, 58] and are high enough for the distance to reattachment to be independent of Re [43, 46, 59]. Moreover, these Reynolds

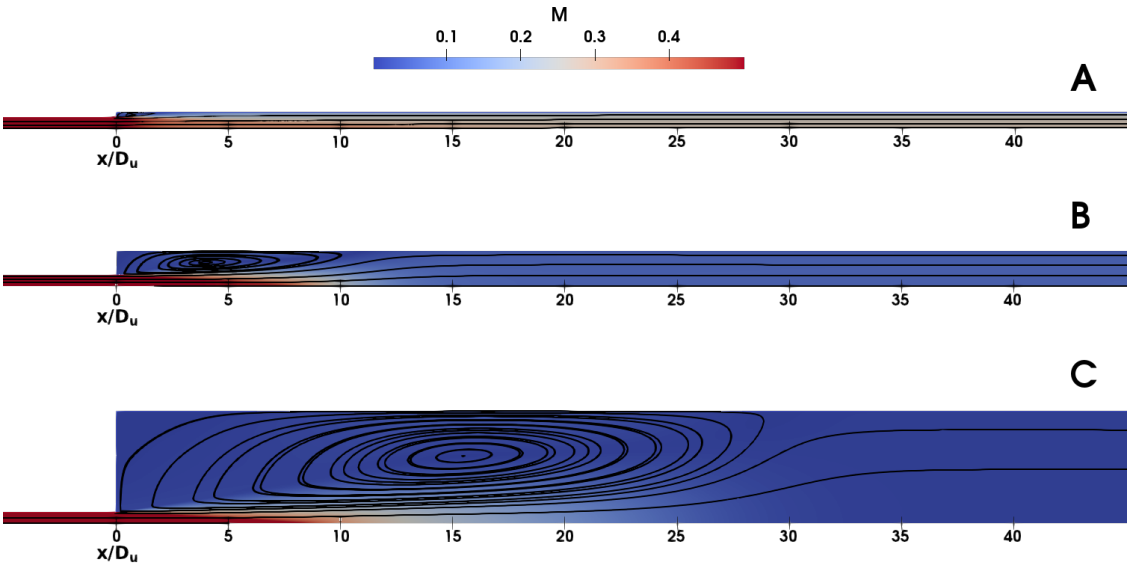

Fig. 3 Local Mach number for an upstream Mach number $M_u = 0.5$ and for various cross section area ratios. (A) $\theta = 0.5$. (B) $\theta = 0.1$. (C) $\theta = 0.01$. Streamlines are represented in black.

numbers ensure that the mean flow topology is the same for all nine cases. This is clearly visible in Fig. 3 which shows the local Mach number and associated streamlines for the large, medium, and small area expansions and for an upstream Mach number $M_u = 0.5$. Similar figures are obtained for lower $M_u = 0.1$ and larger $M_u = 0.9$ Mach numbers. For all nine cases, the turbulent shear layer first detaches from the rim of the sudden area expansion and grows in the axial direction by entraining fluid from both the potential core and the outer recirculation bubbles. The shear layer slightly bends towards the wall due to a small pressure difference between the potential core and the recirculation bubbles, until it finally reattaches at a certain distance x_f from the area expansion. The dimensionless distance to reattachment x_f/H is equal to 10.24 (respectively 9.75) for $\theta = 0.1$ (respectively $\theta = 0.5$), which is in good agreement with previous experimental studies [42, 44–46, 58]. For the largest area expansion with $\theta = 0.01$, the reattachment distance is found to be $x_f/H = 6.54$. These distances are unchanged for lower $M_u = 0.1$ or larger $M_u = 0.9$ Mach numbers.

The mean flow velocity, pressure, temperature, density, turbulent kinetic energy and specific rate of dissipation are further represented in Fig. 4 for the medium area expansion ($\theta = 0.1$) sustaining a moderate Mach number flow ($M_u = 0.5$). The mean temperature (respectively the mean density) suddenly increases (respectively decreases) across the shear layer. This is due to an increase in the mean entropy across the shear layer, which is itself due to viscous dissipation [60]. Conversely, the mean pressure slowly recovers after the area expansion over a distance of about $15D_u$, roughly corresponding to the length of the recirculation bubble.

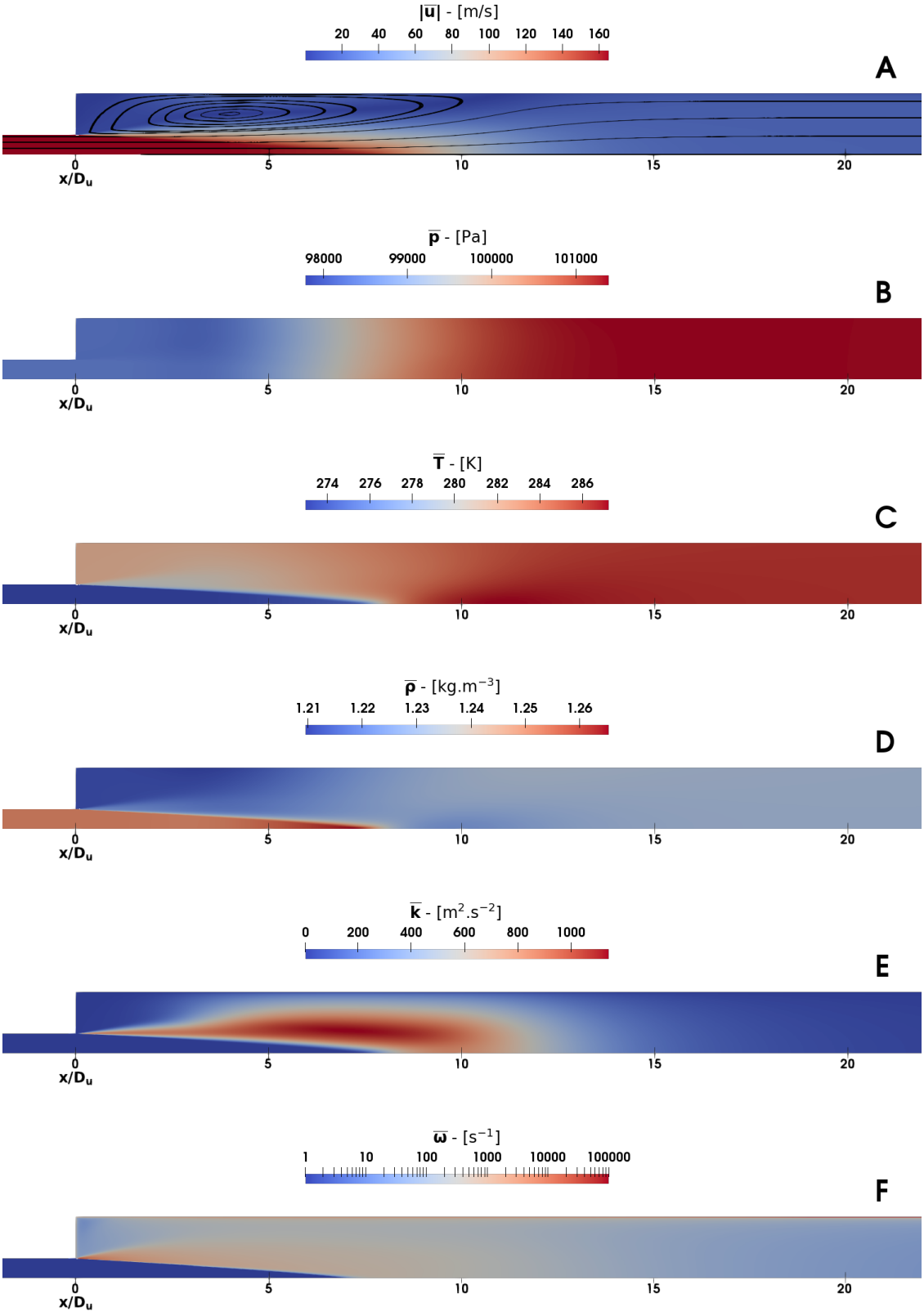

Fig. 4 Mean flow variables for an upstream Mach number $M_u = 0.5$ and a cross section area ratio $\theta = 0.1$. (A) Magnitude of the mean velocity in m/s and associated streamlines. (B) Mean pressure in Pa. (C) Mean temperature in K. (D) Mean density in kg/m^3. (E) Turbulent kinetic energy in m^2/s^2. (F) Specific rate of dissipation in 1/s.

		θ		
		0.01	**0.1**	**0.5**
	0.1	1.0000	1.0000	1.0001
$\mathbf{M_u}$	**0.5**	1.0006	1.0008	1.0015
	0.9	1.0025	1.0029	1.0066

Table 2 Numerical values of $K = \overline{p}_u/\overline{p}_b$ for each configuration of interest.

The quasi-steady analytical model presented in Sec. II is based on the assumption that the pressure acting on the backplate is equal to the pressure just before the area expansion [3, 8, 9, 41]. The accuracy of this typical assumption will now be investigated. For all nine configurations, the mean pressure at $x/D_u = -0.5$ is extracted from the RANS simulations and averaged over the cross section area. The same operation is performed for the backplate pressure and the ratio $K = \overline{p}_u/\overline{p}_b$ is computed for each configuration. The corresponding results are summarised in Tab. 2. The difference between the mean pressure at $x/D_u = -0.5$ and the mean backplate pressure is negligible for a large area expansion with $\theta = 0.01$ sustaining a low Mach number flow with $M_u = 0.1$. This difference then increases for increasing upstream Mach numbers M_u and cross section area ratios θ but remains lower than 0.7% for all cases investigated. The assumption that the backplate pressure is equal to the upstream pressure just before the area expansion is therefore validated. It is also worth noting that K is slightly larger than one for all cases investigated, which is consistent with the presence of a curved shear layer attributed to a slight pressure deficit in the recirculation bubbles.

The predictions according to the mean conservation equations introduced in Sec. II.A are now compared with the numerical results obtained from RANS simulations. The upstream (respectively downstream) numerical flow field variables are assessed at $x/D_u = -20$ (respectively $x/D_u = +40$) and averaged over the cross section area. The numerical values of the downstream Mach number M_d, mean pressure ratio α and mean sound speed ratio Ξ are then computed. Equations (4)-(6) are solved for the same cross section area ratios and for upstream Mach numbers spanning from 0 to 1. Figure 5 depicts the evolution of M_d, α and Ξ with the upstream Mach number M_u for these different cross section area ratios. The match between the analytical predictions and the numerical simulations is excellent for the large ($\theta = 0.01$) and medium ($\theta = 0.1$) area expansions whatever the upstream Mach number and for the narrow ($\theta = 0.5$) area expansion with low-to-moderate upstream Mach numbers ($M_u \leq 0.5$). For the narrow area expansion with a high upstream Mach number ($M_u = 0.9$), the match is still good with a deviation between the numerical simulations and the analytical model of about 5% (respectively $\leq 1.5\%$) for α (respectively M_d and Ξ). The portion of the analytical model describing the evolution of the mean flow variables is thus validated for the wide range of expansion ratios and Mach numbers investigated in this study.

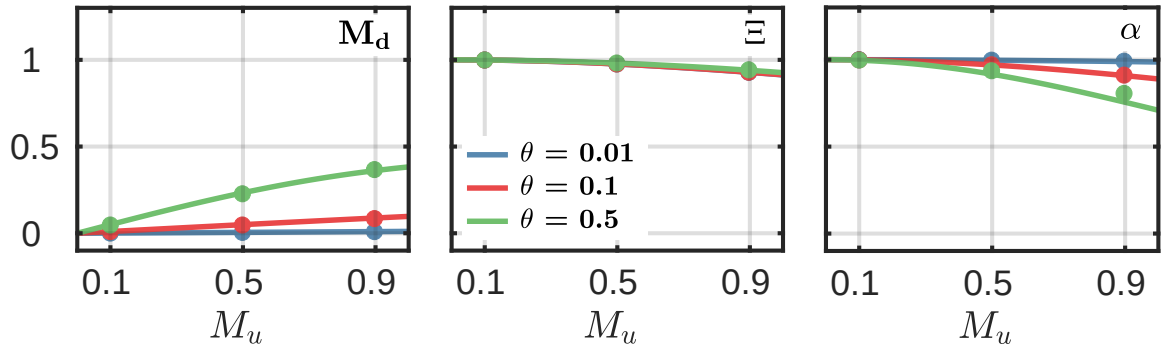

Fig. 5 Downstream Mach number (Left), mean sound speed ratio (Middle) and mean pressure ratio (Right) as functions of the upstream Mach number for three different cross section area ratios. (Blue) $\theta = 0.01$**. (Red)** $\theta = 0.1$**. (Green)** $\theta = 0.5$**. The solid lines represent the predictions according to Eqs. (4)-(6) while the dots represent the numerical values.**

B. Linearised flow simulations

The acoustic response of all nine area expansions is then investigated numerically using two in-house Linearised Navier-Stokes Equations (LNSE) solvers: the coupled solver accounts for the coupling between acoustic and entropy fluctuations while the uncoupled solver assumes that these perturbations are decoupled. Both solvers are 2D axisymmetric compressible solvers in the frequency domain based on second-order Finite Elements. A density-weighted triple decomposition, well adapted to the study of turbulent compressible flows, is employed for both solvers [61]. High-Mach number linearised flow simulations are made possible by the use of a $k-\omega$ SST turbulence model. Turbulence is assumed to be unaffected by deterministic fluctuations such that the eddy viscosity is equal to the value obtained for the mean flow. The linearised conservation of energy is solved in addition to the linearised conservation of mass and momentum in the coupled solver. Entropy fluctuations may thus be generated or damped inside the domain in that case. Conversely, the linearised conservation of energy is replaced by the expression $Ds'/Dt = 0$ in the uncoupled solver. Entropy fluctuations may be convected through the domain but may not be generated or damped in that case. Used jointly, the coupled and uncoupled solvers can thus be used to assess the impact of entropy fluctuations on the acoustic response of area expansions. A Galerkin/Least-Squares formulation (G/LS) is also employed for both solvers. The Least-Squares (LS) method is used to stabilise the solvers as per previous studies [26, 62, 63]. The incoming Riemann invariants at the inlet and outlet can be set to any complex value. More information about these solvers and their validation can be found in [32].

The 2D computational domain is a sequence of two rectangles corresponding to the planar projection of the domain employed for the mean flow simulations. Three unstructured meshes consisting of about 400, 000 triangular elements are optimised for each cross section area ratio θ. More elements are used close to the backplate, separation point, and boundary layer in the downstream duct. The same mesh is employed for all inlet Mach numbers M_u for a given geometry. The normal velocity fluctuations (respectively all components of the velocity fluctuations) are set to zero on the upsteam

lateral wall (respectively on the remaining walls). The acoustic boundary condition is set in terms of incoming Riemann invariants at the inlet and outlet of the computational domain. The inlet is located at $x/D_u = -20$ while the outlet is located at $x/D_u = +40$. Any arbitrary acoustic reflection coefficient located just before ($\mathcal{R}_u$) or just after ($\mathcal{R}_d$) the area expansion may be obtained by properly choosing these incoming Riemann invariants at the inlet and outlet of the computational domain. The Helmholtz number based on the radius of the upstream duct is set to He = 0.007 for all runs unless otherwise stated. This ensures that the sudden area expansion is acoustically and hydrodynamically compact (for the range of Mach numbers investigated in this study). Finally, the incoming entropy s'_u and vorticity $\mathbf{\Omega}'_u$ fluctuations are both set to zero for all runs.

The magnitude of the fluctuating pressure, velocity, entropy, and vorticity is represented in Fig. 6 for $M_u = 0.5$ and $\theta = 0.1$ according to the coupled solver. The associated Riemann invariant at the inlet (respectively outlet) is $f = 100$ Pa (respectively $g = 0$ Pa). Figure 6 shows that plane waves are essentially recovered at a downstream distance $x/D_u \sim 20$. This result was checked to hold for other inlet Mach numbers and acoustic boundary conditions but depends on the cross section area ratio. Furthermore, the pressure fluctuations are continuous across the sudden area expansion, as expected from the literature [8, 9, 30]. This observation, which holds for all cases explored, validates the assumption that the pressure fluctuations on the backplate and just before the area expansion are equal. Figure 6 also confirms that both entropy and vorticity fluctuations are generated by acoustic waves impinging on a sudden area expansion sustaining a subsonic flow [4, 7, 9]. When the uncoupled LNSE solver is employed, vorticity fluctuations are still generated across the area expansion, but not entropy fluctuations since the linearised conservation of energy is not solved in that case.

The coupled and uncoupled LNSE simulations are then used to extract the numerical S-matrix for all cases explored. For each simulation, the two incoming Riemann invariants are imposed on each side of the domain. The complex pressure wave in the upstream (respectively downstream) duct is then reconstructed for $-18 \leq x/D_u \leq -5$ (respectively $25 \leq x/D_u \leq 38$) using the Multi-Microphone Method [64, 65] and propagated to the location of the sudden area expansion. Since the S-matrix has four distinct coefficients, two simulations with independent acoustic boundary conditions at the inlet/outlet are needed to reconstruct the S-matrix for each case and each solver [66–68].

The analytical S-matrix obtained following Ronneberger's approach and the corresponding numerical results according to the coupled and uncoupled solvers are represented in Fig. 7. The imaginary parts of the coefficients of the S-matrix are at least two orders of magnitude smaller than the corresponding real parts and are thus neglected here. The coefficients of the S-matrix according to the coupled and uncoupled solvers are equivalent for $M_u \leq 0.5$ whatever θ. Conversely, discrepancies between the results according to these two solvers can be observed for $M_u = 0.9$, especially when $\theta = 0.5$. It is thus concluded that the acoustic response of the area expansion to incoming acoustic waves is not

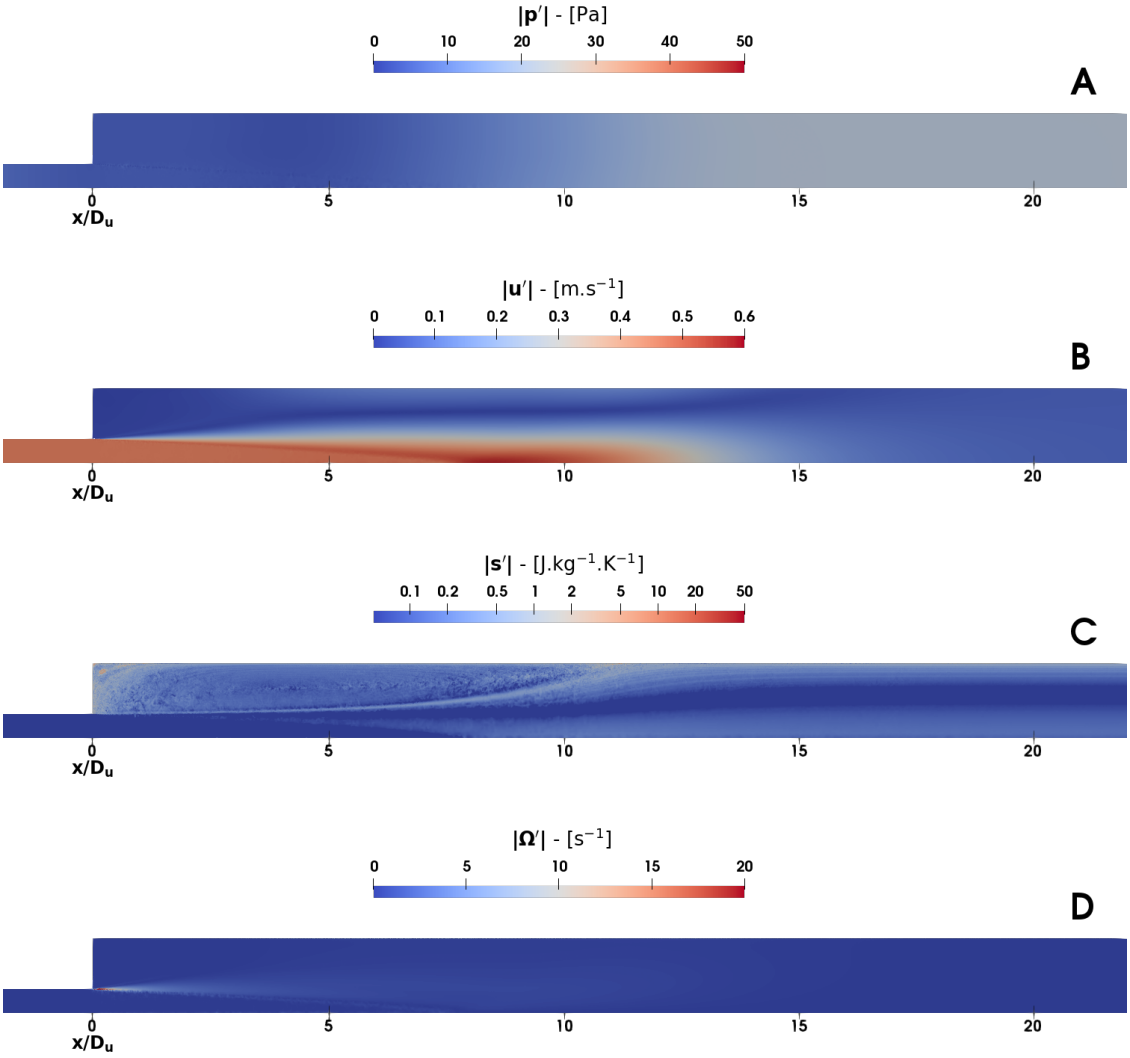

Fig. 6 Fluctuating variables for an upstream Mach number $M_u = 0.5$, a cross section area ratio $\theta = 0.1$ and $f = 100$ Pa obtained using the coupled LNSE solver. (A) Magnitude of the fluctuating pressure in Pa. (B) Magnitude of the fluctuating velocity in m/s. (C) Magnitude of the fluctuating entropy in J/(kg.K). (D) Magnitude of the fluctuating vorticity in 1/s.

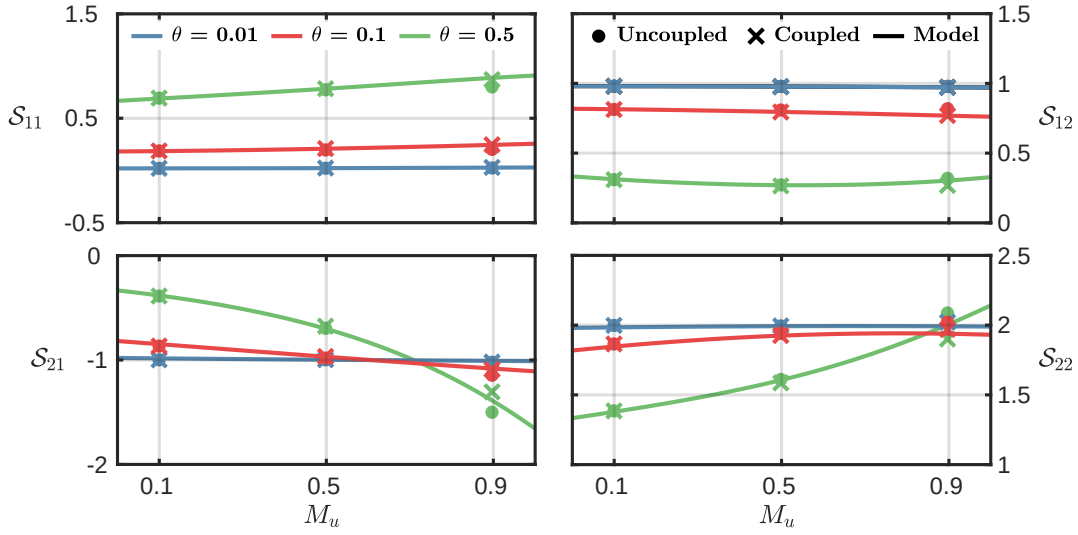

Fig. 7 Coefficients of the S-matrix as functions of the upstream Mach number for three different cross section area ratios. (Blue) $\theta = 0.01$**. (Red)** $\theta = 0.1$**. (Green)** $\theta = 0.5$**. The solid lines represent the analytical predictions. The dots and crosses represent the numerical values obtained using the uncoupled and coupled LNSE solvers respectively.**

affected by entropy fluctuations at low and intermediate inlet Mach numbers. As the Mach number increases, entropy fluctuations then have an increasingly large influence on the coefficients of the S-matrix. Figure 7 also demonstrates that the agreement between the analytical S-matrix and the corresponding numerical results is excellent, especially with the coupled solver.

The numerical acoustic absorption coefficient is now computed using Eq. (13b) along with the numerical S-matrices according to the coupled and uncoupled solvers. The numerical acoustic absorption coefficient is also computed directly from the incoming and outgoing Riemann invariants using Eq. (13a) for a number of mean flow parameters and acoustic boundary conditions. Both approaches lead to the same value for the acoustic absorption coefficient (within a small numerical tolerance) but the former is retained in this study. The numerical acoustic absorption coefficients are represented in Fig. 8 as functions of the modulus and phase of the upstream acoustic reflection coefficient for all nine cases of interest. The left (respectively right) plot in each subfigure represents the numerical results according to the coupled (respectively uncoupled) solver. The numerical absorption coefficients according to the coupled and uncoupled solvers are found to be equivalent for $M_u \leq 0.5$ whatever θ. The damping of acoustic energy across sudden area expansions is thus unaffected by the presence of entropy fluctuations at low and intermediate Mach numbers. Conversely, for a medium ($\theta = 0.1$) or small ($\theta = 0.5$) area expansion with $M_u = 0.9$, some deviations appear between the acoustic absorption coefficients obtained with the coupled and uncoupled solvers. A notable

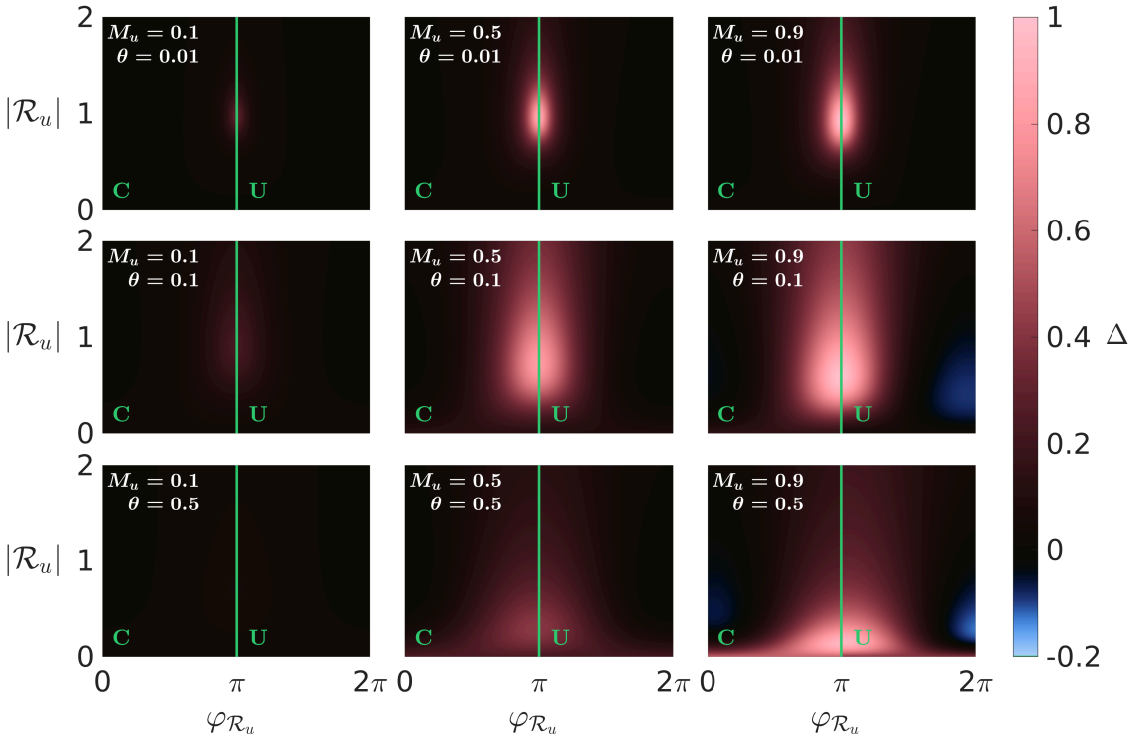

Fig. 8 Numerical acoustic absorption coefficient of a sudden area expansion as a function of the modulus (y-axis) and phase (x-axis) of the upstream acoustic reflection coefficient for three different upstream Mach numbers and cross section area ratios. (Top) $\theta = 0.01$**. (Center)** $\theta = 0.1$**. (Bottom)** $\theta = 0.5$**. (Left)** $M_u = 0.1$**. (Middle)** $M_u = 0.5$**. (Right)** $M_u = 0.9$**. The left (respectively right) part of each subplot is obtained using the coupled (respectively uncoupled) Linearised Navier-Stokes Equation solver. Acoustic energy is generated for** $\Delta < 0$ **corresponding to a blue hue.**

difference is found for $\mathcal{R}_u \sim 0.5$, corresponding to a significant amount of acoustic energy generation across the sudden area expansion according to the uncoupled solver while the coupled solver predicts a more limited amount of acoustic energy generation. It is thus concluded that the presence of entropy fluctuations has a significant impact on acoustic energy generation across sudden area expansions sustaining high Mach number flows. Furthermore, the numerical results according to both the coupled and uncoupled solvers are in excellent agreement with the analytical predictions at low and intermediate Mach numbers, as can be seen by comparing Fig. 2 with Fig. 8. At high Mach numbers, the uncoupled solver fails because entropy fluctuations are not allowed to be generated inside the domain, which violates the conservation of energy. The best match is thus obtained for the coupled solver at high Mach numbers. The quasi-steady analytical model presented in Sec. II is thus validated for the wide range of geometries, mean flow parameters and acoustic boundary conditions investigated in this study. This includes high subsonic Mach numbers, which had not been investigated in previous studies. Finally, the presence of regions where $\Delta < 0$ is confirmed by these numerical simulations, which demonstrates that sudden area expansions may experience whistling for specific sets of parameters $(M_u, \theta, \mathcal{R}_u)$. Since there are no incoming entropy s'_u and vorticity $\mathbf{\Omega}'_u$ fluctuations in either the analytical model or the LNSE simulations, this acoustic energy surplus is necessarily extracted from the mean flow.

These observations can be used to design sudden area expansions with optimal damping properties. For large area expansions with $\theta \ll 1$, a moderate or high Mach number flow will damp most of the acoustic energy for an upstream acoustic boundary condition close to that of an open end ($\mathcal{R}_u \sim -1$). For small sudden area expansions with $\theta \sim 1$, a high Mach number flow is required to obtain a similar amount of acoustic energy damping. In that case, the upstream acoustic reflection coefficient must be considered carefully as acoustic energy generation will occur for specific ranges of $\mathcal{R}_u$.

C. Linearised flow simulations at finite frequencies

The quasi-steady analytical model used in this work has been validated numerically for a very low Helmholtz number He = 0.007 but its applicability at higher frequencies is also of interest. Consequently, the S-matrices of a large ($\theta = 0.01$), medium ($\theta = 0.1$) and small ($\theta = 0.5$) area expansion sustaining a moderate ($M_u = 0.5$) Mach number flow are determined using the coupled LNSE solver for increasingly large Helmholtz numbers and compared with the quasi-steady analytical predictions. Since the value of the inlet Mach number is prescribed for all simulations presented in this section, the Strouhal and Helmholtz numbers can be used interchangeably, but the latter is used here. It should be noted that the coefficients of the S-matrices become complex as the frequency is increased [9, 25, 27]. Figures 9-10 represent the moduli and phases of the four coefficients of these S-matrices as functions of the Helmholtz number. The quasi-steady analytical predictions are depicted as arrows in these figures. Figures 9-10 demonstrate that the moduli and phases of all four coefficients of the S-matrices remain close to their quasi-steady value for Helmholtz numbers up

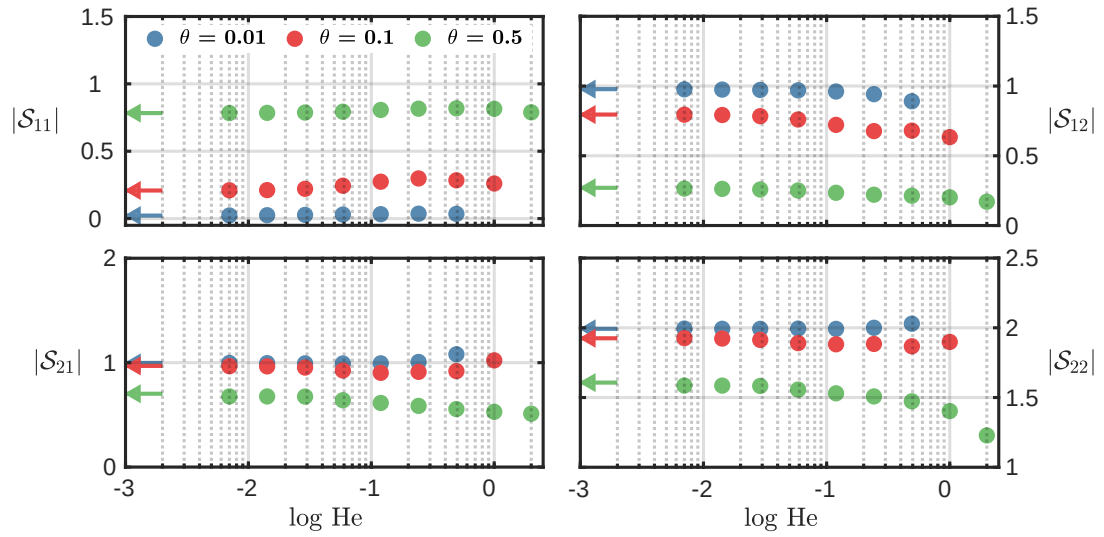

Fig. 9 Modulus of the coefficients of the S-matrix as functions of the Helmholtz number for three different cross section area ratios and for $M_u = 0.5$. (Blue) $\theta = 0.01$. (Red) $\theta = 0.1$. (Green) $\theta = 0.5$. The dots represent the numerical values obtained using the coupled solver. The arrows represent the quasi-steady analytical predictions.

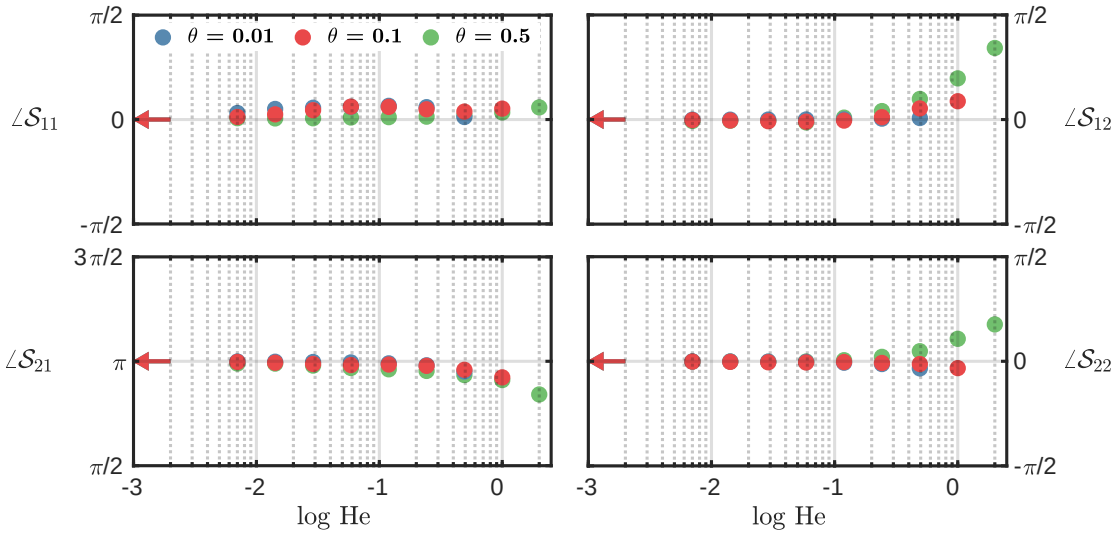

Fig. 10 Phase of the coefficients of the S-matrix as functions of the Helmholtz number for three different cross section area ratios and for $M_u = 0.5$. (Blue) $\theta = 0.01$. (Red) $\theta = 0.1$. (Green) $\theta = 0.5$. The dots represent the numerical values obtained using the coupled solver. The arrows represent the quasi-steady analytical predictions.

to He $\sim 0.05 - 0.1$, thus providing an upper validity limit for the quasi-steady analytical model. A large number of industrial configurations, including exhaust systems [3, 4], engine intakes [3], and gas turbine combustors [5, 68] fall under this frequency limit.

IV. Main conclusions

The acoustic energy balance of sudden cross section area expansions sustaining a high Reynolds number subsonic mean flow is of interest to predict the thermoacoustic stability of gas turbines and the efficiency of car mufflers, among others. The objective of this study was to investigate the damping and generation of acoustic energy across sudden area expansions for a large spectrum of geometries, mean flows, and acoustic boundary conditions using numerical tools as well as an analytical model based on Ronneberger's quasi-steady approach. This was achieved by considering the acoustic absorption coefficient Δ of various sudden area expansions, acoustic energy being generated (respectively damped) for $\Delta < 0$ (respectively $\Delta > 0$). The analytical acoustic absorption coefficient was shown to be a function of two mean flow parameters (e.g. the inlet Mach number M_u and cross section area ratio θ) and one acoustic boundary condition (e.g. the upstream acoustic reflection coefficient $\mathcal{R}_u$). The impact of the upstream reflection coefficient was found to be increasingly important as the Mach number was increased. For small area expansions sustaining a high Mach number flow, the acoustic absorption coefficient was found to range between slightly negative values (limited acoustic energy generation, corresponding to a whistling configuration) to almost one (total acoustic energy damping) depending on the specific value of $\mathcal{R}_u$.

These analytical predictions were then examined using a two-step numerical stategy. Nine reference cases, corresponding to a large ($\theta = 0.01$), medium ($\theta = 0.1$) and small ($\theta = 0.5$) area expansion sustaining a low ($M_u = 0.1$), moderate ($M_u = 0.5$) and high ($M_u = 0.9$) Mach number flow were first defined. The mean flow variables corresponding to these reference cases were then obtained using RANS simulations with a $k - \omega$ SST turbulence model. The mean flow topology was found to be correctly captured by these RANS simulations. The mean pressure on the backplate and just before the sudden area expansion were found to be the same within 0.7% for all cases investigated. Finally, the agreement between the RANS simulations and the equations describing the mean flow in the model was found to be excellent. Two in-house Linearised Navier-Stokes Equations solvers were then used to characterise the acoustic response of the area expansion to incoming acoustic waves for all nine reference cases. A density-weighted triple decomposition along with a $k - \omega$ SST turbulence model were used in both solvers, thus making them well adapted to high-Mach number flow simulations. Vorticity fluctuations were allowed to be generated and damped inside the domain in the coupled and uncoupled solvers, but not entropy fluctuations, which were only allowed in the former. The Helmholtz number based on the radius of the upstream duct was set to He = 0.007. The numerical results according to both solvers were found to

be equivalent for $M_u \leq 0.5$ but not for $M_u = 0.9$, thus indicating that the impact of entropy fluctuations on the acoustic response of sudden area expansions becomes important at high Mach numbers. The agreement between the analytical S-matrices and their numerical counterparts was found to be excellent for all parameters investigated, especially with the coupled solver. The numerical acoustic absorption coefficient according to the coupled solver was also shown to be in excellent agreement with the analytical model whatever $(M_u, \theta, \mathcal{R}_u)$. It was also confirmed numerically that specific values of $\mathcal{R}_u$ lead to acoustic energy generation across small sudden area expansions sustaining a high Mach number flow, thus indicating that these configurations are prone to whistling. The acoustic energy surplus is extracted from the mean flow in that case. Conversely, large sets of parameters $(M_u, \theta, \mathcal{R}_u)$ were found to be associated with considerable amounts of acoustic energy damping across the area expansion. Finally, the damping and generation of acoustic energy across sudden area expansions was investigated numerically as the Helmholtz number was increased. It was found that the quasi-steady analytical model was accurate up to $\mathrm{He} \sim 0.1$, thus covering a broad range of industrial applications.

Funding Sources

The authors would like to gratefully acknowledge the European Research Council (ERC) Consolidator Grant AFIRMATIVE (2018–2023, grant number 772080) for supporting this research.

References

[1] Boij, S., and Nilsson, B., "Reflection of sound at area expansions in a flow duct," *J. Sound Vib.*, Vol. 260, No. 3, 2003, pp. 477–498.

[2] Munjal, M. L., *Acoustics of ducts and mufflers*, John Wiley and Sons, Inc., New York, 1987.

[3] Davies, P. O. A. L., "Practical flow duct acoustics," *J. Sound Vib.*, Vol. 124, No. 1, 1988, pp. 91–115.

[4] Alfredson, R. J., and Davies, P. O. A. L., "Performance of exhaust silencer components," *J. Sound Vib.*, Vol. 15, No. 2, 1971, pp. 175–196.

[5] Dowling, A. P., and Stow, S. R., "Acoustic analysis of gas turbine combustors," *J. Propul. Power*, Vol. 19, No. 5, 2003, pp. 751–764.

[6] Gaudron, R., Yang, D., and Morgans, A. S., "Acoustic energy balance during the onset, growth and saturation of thermoacoustic instabilities," *J. Eng. Gas Turbines Power*, 2020.

[7] Ronneberger, D., "Experimentelle Untersuchungen zum akustischen Reflexionsfaktor von unstetigen Querschnittsänderungen in einem luftdurchströmten Rohr," *Acustica*, Vol. 19, 1967, pp. 222 – 235.

[8] Cummings, A., "Sound transmission at sudden area expansions in circular ducts, with superimposed mean flow," *J. Sound Vib.*, Vol. 38, No. 1, 1975, pp. 149–155.

[9] Ronneberger, D., "Theoretische und experimentelle Untersuchung der Schallausbreitung durch Querschnittssprünge und Lochplatten in Strömungskanälen," Tech. rep., Drittes Physikalisches Institut der Universität Göttingen, 1987.

[10] Cummings, A., and Haddad, H., "Sudden area changes in flow ducts: Further thoughts," *J. Sound Vib.*, Vol. 54, No. 4, 1977, pp. 611–612.

[11] Chu, B. T., and Kovasznay, L. S. G., "Non-linear interactions in a viscous heat-conducting compressible gas," *J. Fluid Mech.*, Vol. 3, No. 5, 1958, pp. 494–514.

[12] Rayleigh, B., *The theory of sound - volume I*, Macmillan and Co., London, 1877.

[13] Lieuwen, T. C., *Unsteady combustor physics*, Cambridge University Press, 2005.

[14] Myers, M. K., "Transport of energy by disturbances in arbitrary steady flows," *J. Fluid Mech.*, Vol. 226, 1991, pp. 383–400.

[15] Ronneberger, D., "Zur Kutta-Bedingung bei der Schallausbreitung durch durchströmte Querschnittssprünge und Lochplatten," *Fortschritte der Akustik DAGA'89*, Duisburg, 1989.

[16] Dupère, I. D. J., and Dowling, A. P., "The absorption of sound near abrupt axisymmetric area expansions," *J. Sound Vib.*, Vol. 239, No. 4, 2001, pp. 709–730.

[17] Kooijman, G., Testud, P., Aurégan, Y., and Hirschberg, A., "Multimodal method for scattering of sound at a sudden area expansion in a duct with subsonic flow," *J. Sound Vib.*, Vol. 310, No. 4-5, 2008, pp. 902–922.

[18] Yanaz Çınar, Ö., Boij, S., Çınar, G., and Nilsson, B., "Sudden area expansion in ducts with flow – A comparison between cylindrical and rectangular modelling," *J. Sound Vib.*, Vol. 396, 2017, pp. 307–324.

[19] Yang, D., and Morgans, A. S., "A semi-analytical model for the acoustic impedance of finite length circular holes with mean flow," *J. Sound Vib.*, Vol. 384, 2016, pp. 294–311.

[20] Yang, D., and Morgans, A. S., "The acoustics of short circular holes opening to confined and unconfined spaces," *J. Sound Vib.*, Vol. 393, 2017, pp. 41–61.

[21] Boij, S., and Nilsson, B., "Scattering and absorption of sound at flow duct expansions," *J. Sound Vib.*, Vol. 289, No. 3, 2006, pp. 577–594.

[22] Dupère, I. D. J., and Dowling, A. P., "Absorption of sound near abrupt area expansions," *AIAA J.*, Vol. 38, No. 2, 2000, pp. 193–202.

[23] Kooijman, G., Hirschberg, A., and Aurégan, Y., "Influence of mean flow profile and geometrical ratios on scattering of sound at a sudden area expansion in a duct," *J. Sound Vib.*, Vol. 329, No. 5, 2010, pp. 607–626.

[24] Lambert, R. F., and Steinbrueck, E. A., "Acoustic synthesis of a flowduct area discontinuity," *J. Acoust. Soc. Am.*, Vol. 67, No. 1, 1980, pp. 59–65.

[25] Peerlings, L., Boij, S., and Bodén, H., "Experimental investigation of the aero-acoustic interaction at an area-expansion," *J. Sound Vib.*, 2019.

[26] Gikadi, J., Schulze, M., Schwing, J., Foeller, S., and Sattelmayer, T., "Linearized Navier-Stokes and Euler equations for the determination of the acoustic scattering behaviour of an area expansion," *33rd AIAA Aeroacoustics Conference*, 2012.

[27] Föller, S., and Polifke, W., "Identification of aero-acoustic scattering matrices from large eddy simulation. Application to a sudden area expansion of a duct," *J. Sound Vib.*, Vol. 331, No. 13, 2012, pp. 3096–3113.

[28] Kierkegaard, A., Boij, S., and Efraimsson, G., "Simulations of the scattering of sound waves at a sudden area expansion," *J. Sound Vib.*, Vol. 331, No. 5, 2012, pp. 1068–1083.

[29] Peerlings, L., "Assessing precision and accuracy in acoustic scattering matrix measurements," Ph.D. thesis, 2017.

[30] Gentemann, A., Fischer, A., Evesque, S., and Polifke, W., "Acoustic transfer matrix reconstruction and analysis for ducts with sudden change of area," *9th AIAA/CEAS Aeroacoustics Conference and Exhibit, May 12-14, 2003, Hilton Head, South Carolina*, 2003, pp. 1–11.

[31] Yang, D., Guzmán-Iñigo, J., and Morgans, A. S., "Sound generation by entropy perturbations passing through a sudden flow expansion," *J. Fluid Mech.*, Vol. 905, No. R2, 2020.

[32] Guzmán-Iñigo, J., Yang, D., Gaudron, R., and Morgans, A. S., "On the scattering of acoustic and entropy waves at sudden area expansions," *Submitted to J. Sound Vib.*, 2021.

[33] Marble, F. E., and Candel, S. M., "Acoustic disturbance from gas non-uniformities convected through a nozzle," *J. Sound Vib.*, Vol. 55, No. 2, 1977, pp. 225–243.

[34] Gaudron, R., and Morgans, A. S., "Acoustic absorption in a subsonic mean flow at a sudden cross section area change," *Proc. Int. Cong. Sound Vib. (ICSV26)*, 2019, pp. 1–8.

[35] Dowling, A. P., and Morgans, A. S., "Feedback control of combustion oscillations," *Annu. Rev. Fluid Mech.*, Vol. 37, No. 1, 2005, pp. 151–182.

[36] Cantrell, R. H., and Hart, R. W., "Interaction between sound and flow in acoustic cavities: mass, momentum, and energy considerations," *J. Acous. Soc. Am.*, Vol. 36, No. 4, 1964, pp. 697–706.

[37] Morfey, C. L., "Acoustic energy in non-uniform flows," *J. Sound Vib.*, Vol. 14, No. 2, 1971, pp. 159–170.

[38] Durox, D., Schuller, T., Noiray, N., Birbaud, A. L., and Candel, S., "Rayleigh criterion and acoustic energy balance in unconfined self-sustained oscillating flames," *Combust. Flame*, Vol. 156, No. 1, 2009, pp. 106–119.

[39] Aurégan, Y., and Starobinski, R., "Determination of acoustical energy dissipation/production potentiality from the acoustical transfer functions of a multiport," *Acustica*, Vol. 85, No. 6, 1999, pp. 788–792.

[40] Testud, P., Aurégan, Y., Moussou, P., and Hirschberg, A., "The whistling potentiality of an orifice in a confined flow using an energetic criterion," *J. Sound Vib.*, Vol. 325, No. 4-5, 2009, pp. 769–780.

[41] Batchelor, G. K., *An Introduction to fluid dynamics*, Cambridge University Press, 1967.

[42] Moon, L. F., and Rudinger, G., "Velocity distribution in an abruptly expanding circular duct," *J. Fluid Eng.*, 1977, pp. 226–230.

[43] Devenport, W. J., "Separation bubbles at high Reynolds number: measurement and computation," Ph.D. thesis, University of Cambridge, 1985.

[44] Durrett, R. P., Stevenson, W. H., and Thompson, H. D., "Radial and axial turbulent flow measurements with an LDV in an axisymmetric sudden expansion air flow," *J. Fluid Eng.*, Vol. 110, 1988, pp. 367–372.

[45] Gould, R. D., Stevenson, W. H., and Thompson, H. D., "Investigation of turbulent transport in an axisymmetric sudden expansion," *AIAA J.*, Vol. 28, No. 2, 1990, pp. 276–283.

[46] Devenport, W. J., and Sutton, E. P., "An experimental study of two flows through an axisymmetric sudden expansion," *Exp. Fluids*, Vol. 14, No. 6, 1993, pp. 423–432.

[47] Guo, B., Langrish, T. A. G., and Fletcher, D. F., "Numerical simulation of unsteady turbulent flow in axisymmetric sudden expansions," *J. Fluid Eng.*, Vol. 123, 2001.

[48] Afshari, A., Jaberi, F. A., and Shih, T. I., "Large-eddy simulations of turbulent flows in an axisymmetric dump combustor," *AIAA J.*, Vol. 46, No. 7, 2008, pp. 1576–1592.

[49] Rienstra, S. W., and Hirschberg, A., *An Introduction to acoustics*, 2017.

[50] Bechert, D. W., "Sound absorption caused by vorticity shedding, demonstrated with a jet flow," *J. Sound Vib.*, Vol. 70, No. 3, 1980, pp. 389–405.

[51] Howe, M. S., "Contributions to the theory of aerodynamic sound, with application to excess jet noise and the theory of the flute," *J. Fluid Mech.*, Vol. 71, No. 4, 1975, pp. 625–673.

[52] Hirschberg, A., and Rienstra, S. W., *An introduction to aeroacoustics*, 2004.

[53] Pierce, A. D., *Acoustics - An introduction to its physical principles and applications*, 1980.

[54] Su, J., Rupp, J., Garmory, A., and Carrotte, J. F., "Measurements and computational fluid dynamics predictions of the acoustic impedance of orifices," *J. Sound Vib.*, Vol. 352, 2015, pp. 174–191.

[55] Guzmán-Iñigo, J., Yang, D., Johnson, H. G., and Morgans, A. S., "Sensitivity of the acoustics of short circular holes with bias flow to inlet edge geometries," *AIAA J.*, Vol. 57, No. 11, 2019, pp. 4835–4844.

[56] Weller, H. G., Tabor, G., Jasak, H., and Fureby, C., "A tensorial approach to computational continuum mechanics using object-oriented techniques," *Comput. Phys.*, Vol. 12, No. 6, 1998, p. 620.

[57] Menter, F., Kuntz, M., and Langtry, R. B., "Ten years of industrial experience with the SST turbulence model," *Heat Mass Transf.*, Vol. 4, 2003, pp. 625–632.

[58] Stevenson, W. H., Thompson, H. D., and Craig, R. R., "Laser velocimeter measurements in highly turbulent recirculating flows," *J. Fluid Eng.*, Vol. 106, 1984, pp. 173–180.

[59] Simpson, R. L., "Aspects of turbulent boundary-layer separation," *Prog. Aerosp. Sci.*, Vol. 32, No. 5, 1996, pp. 457–521.

[60] Kundu, P. K., Cohen, I. M., and Dowling, D. R., *Fluid mechanics*, 5^{th} ed., Elsevier, 2012.

[61] Alizard, F., Pirozzoli, S., Bernardini, M., and Grasso, F., "Optimal transient growth in compressible turbulent boundary layers," *J. Fluid Mech.*, Vol. 770, 2015, pp. 124–155.

[62] Donea, J., and Huerta, A., *Finite element methods for flow problems*, John Wiley & Sons, Ltd, 2003.

[63] Gikadi, J., Föller, S., and Sattelmayer, T., "Impact of turbulence on the prediction of linear aeroacoustic interactions: Acoustic response of a turbulent shear layer," *J. Sound Vib.*, Vol. 333, No. 24, 2014, pp. 6548–6559.

[64] Chung, J. Y., and Blaser, D. A., "Transfer function method of measuring in-duct acoustic properties. I. Theory," *J. Acoust. Soc. Am.*, Vol. 68, 1980, pp. 907–913.

[65] Jang, S.-H., and Ih, J.-G., "On the multiple microphone method for measuring in-duct acoustic properties in the presence of mean flow," *J. Acous. Soc. Am.*, Vol. 103, No. 3, 1998, pp. 1520–1526.

[66] Åbom, M., "A note on the experimental determination of acoustical two-port matrices," *J. Sound Vib.*, Vol. 155, No. 1, 1992, pp. 185–188.

[67] Paschereit, C. O., and Polifke, W., "Investigation of the thermoacoustic characteristics of a lean premixed gas turbine burner - 98-GT-582," *Proc. ASME Turbo Expo 1998*, 1998, pp. 1–10.

[68] Merk, M., Silva, C., Polifke, W., Gaudron, R., Gatti, M., Mirat, C., and Schuller, T., "Direct assessment of the acoustic scattering matrix of a turbulent swirl combustor by combining system identification, Large Eddy Simulation and analytical approaches," *J. Eng. Gas Turbines Power*, Vol. 141, No. 2, 2018, pp. 1–9.